# Zoo3D: Zero-Shot 3D Object Detection at Scene Level

Andrey Lemeshko<sup>1\*</sup>, Bulat Gabdullin<sup>2\*</sup>, Nikita Drozdov<sup>1</sup>, Anton Konushin<sup>1</sup>, Danila Rukhovich<sup>3</sup>, Maksim Kolodiazhnyi<sup>1†</sup>

<sup>1</sup>Lomonosov Moscow State University; <sup>2</sup>Higher School of Economics; 

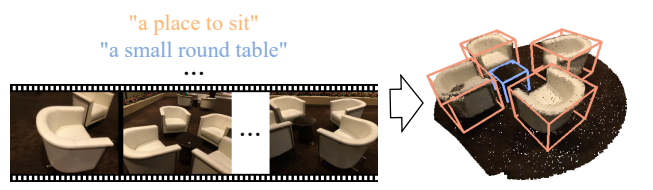
<sup>3</sup>M:3L Lab, Institute of Mechanics, Armenia

## **Abstract**

3D object detection is fundamental for spatial understanding. Real-world environments demand models capable of recognizing diverse, previously unseen objects, which remains a major limitation of closed-set methods. Existing open-vocabulary 3D detectors relax annotation requirements but still depend on training scenes, either as point clouds or images. We take this a step further by introducing Zoo3D, the first training-free 3D object detection framework. Our method constructs 3D bounding boxes via graph clustering of 2D instance masks, then assigns semantic labels using a novel open-vocabulary module with bestview selection and view-consensus mask generation. Zoo3D operates in two modes: the zero-shot Zoo3D<sub>0</sub>, which requires no training at all, and the self-supervised  $Zoo3D_1$ , which refines 3D box prediction by training a class-agnostic detector on Zoo3D<sub>0</sub>-generated pseudo labels. Furthermore, we extend Zoo3D beyond point clouds to work directly with posed and even unposed images. Across Scan-Net200 and ARKitScenes benchmarks, both Zoo3D<sub>0</sub> and  $Zoo3D_1$  achieve state-of-the-art results in open-vocabulary 3D object detection. Remarkably, our zero-shot Zoo3D<sub>0</sub> outperforms all existing self-supervised methods, hence demonstrating the power and adaptability of training-free, off-the-shelf approaches for real-world 3D understanding. Code is available at https://github.com/col14m/ zoo3d.

#### 1. Introduction

3D object detection aims to predict both category labels and oriented 3D bounding boxes for all objects within a scene. Adapting existing detection methods to real-world scenarios is often challenging and resource-intensive: collecting training data and fine-tuning models require substantial time and computational effort. Consequently, self-



Method	S	ScanNet20			
Method	Depths	Images	Poses	Boxes	$mAP_{25}$
OV-Uni3DETR [32]	1	1	1	1	25.3
OpenM3D [7]	✓	✓	/		19.8
$Zoo3D_0$					24.2
$Zoo3D_1$		✓			27.9

Figure 1. Open-vocabulary 3D object detection aims to localize 3D bounding boxes given a textual description. We demonstrate that this task can be solved in a zero-shot mode ( $Zoo3D_0$ ). Our self-supervised image-based approach  $Zoo3D_1$  performs on par with point cloud-based methods that are trained with 3D bounding boxes supervision.

contained, off-the-shelf approaches with minimal supervision are highly desirable.

Fully supervised methods [11, 17, 23, 25, 26], including recent LLM-based variants [15, 18, 42, 43, 45], achieve impressive accuracy in closed-set 3D object detection but fail to generalize beyond training categories. Their performance remains limited by the diversity, size, and quality of annotated datasets. Self-supervised approaches [7, 14, 32, 34] alleviate the need for manual annotations, yet their detection quality still lags behind fully supervised methods. Zero-shot detection represents the next frontier toward supervision-free 3D understanding. While zero-shot techniques have been proposed for related tasks such as 3D instance segmentation [27, 33, 41] and monocular 3D detection [36, 37], multi-view 3D object detection has never been addressed in a truly zero-shot setting. Meanwhile, generalist vision-language models (VLMs) [1, 6] excel at singleview prediction and visual question answering from images or videos, but they still struggle to perform spatial reasoning at the scene level.

In 2D vision, zero-shot approaches [12, 21] leverage

<sup>\*</sup>Equal contribution

<sup>†</sup>Corresponding author: kolodyazhniyma@my.msu.ru

foundation models such as SAM [20] for segmentation and CLIP [19] for visual–textual alignment. These same models have been repurposed for 3D understanding; for example, self-supervised 3D object detectors [7, 34] use CLIP and SAM to generate pseudo-labels during training. However, we ask a more ambitious question: *can we develop a completely training-free 3D object detector?* In this work, we harness the potential of foundation models for training-free 3D understanding and present Zoo3D<sub>0</sub>, the first-in-class zero-shot 3D object detection framework that outperforms existing self-supervised approaches. Moreover, we further improve prediction quality with a self-supervised Zoo3D<sub>1</sub>.

Beyond training supervision, inference requirements also pose challenges. Point clouds—commonly required by 3D understanding methods—are not always available in practice. We overcome this limitation by employing another foundation model, DUSt3R [31], to bridge the gap between 2D and 3D representations. This way, we enable 3D object detection directly from images, which is a step toward democratizing spatial intelligence.

In summary, we investigate how far the requirements for 3D object detection can be relaxed. Starting from point clouds and ground-truth annotations, we progressively reduce supervision and input modality requirements, ultimately introducing a training-free approach that operates directly on unposed images. Even in this most constrained setting, our method performs on par with existing approaches that rely on extensive training and point cloud inputs at inference time. Our contributions are as follows:

- We define a novel task: zero-shot indoor 3D object detection at the scene level.
- We propose novel methods for open-vocabulary 3D object detection in zero-shot and self-supervised settings.
- Our methods achieve state-of-the-art results on four ScanNet-based benchmarks across three input modalities: point clouds, posed images, and unposed images.

#### 2. Related Work

**3D Object Detection from Point Clouds.** Existing methods for 3D object detection from point clouds can be categorized by the level of supervision involved.

Supervised methods, such as FCAF3D [23], TR3D [25], UniDet3D [11], and V-DETR [26], rely on fully annotated 3D bounding boxes. More recently, LLM-based approaches like Video-3D LLM [42], LSceneLLM [43], and Chat-Scene [9] have leveraged multimodal reasoning to enhance semantic understanding, but still are fundamentally constrained by the limited size and diversity of annotated 3D datasets, and cannot generalize beyond seen classes.

Semi-supervised approaches, e.g., OV-Uni3DETR [32], CoDa [3], OV-3DETIC [13], Object2Scene [44], INHA [10], and FM-OV3D [40], are trained on a subset of labeled 3D bounding boxes and evaluated on

both seen and unseen categories in an open-vocabulary mode. These models bridge the gap between closed-set and open-world detection but still rely on training scenes with ground truth boxes.

Self-supervised methods, including OV-3DET [14], ImOV3D [34], and GLIS [16], eliminate the need for explicit 3D labels by generating pseudo-annotations or distilling 2D supervision. Despite reduced supervision, they still require exposure to 3D scenes and rely on suboptimal pseudo-box generation or text-visual alignment strategies. Our method improves this stage via a simplified and training-free pipeline using only CLIP [19] and SAM [20].

Zero-shot approaches do not require any data from training scenes. Outdoor-focused methods such as SAM3D [39] operate on BEV projections but do not generalize to indoor scenes. MaskClustering [33], OnlineAnySeg [27], and SAM2Object [41] address open-vocabulary 3D instance segmentation, yet not 3D object detection. To our knowledge, we are the first to formulate and tackle indoor 3D object detection in the zero-shot regime.

**3D Object Detection from Posed Multi-view Images.** Supervised methods such as ImVoxelNet [24], ImGeoNet [29], and NeRF-Det++ [8] derive closed-vocabulary 3D scene representation with 3D objects from collections of images with corresponding poses. Recent LLM-powered models like LLaVA-3D [45] and GPT4Scene [18] introduce large-scale vision-language understanding but still require labeled training data.

In the open-vocabulary regime, OV-Uni3DETR [32] unifies training across both images and point clouds, while OpenM3D [7] combines CLIP features with voxelized 3D representations. The latter is most related to our approach but depends on depth supervision and CLIP finetuning, whereas we remain entirely training-free and use frozen CLIP features only at inference, yielding stronger performance. No prior methods address zero-shot 3D object detection directly from posed images;  $Zoo3D_0$  is the first-inclass method tackling this task.

#### 3D Object Detection from Unposed Multi-view Images.

The most unconstrained setting, unposed multi-view images, has only recently been explored by LLM-based approaches such as VLM-3R [5] and SpatialLM [15], which require full supervision. No prior work has attempted openvocabulary, self-supervised, or zero-shot 3D object detection in this modality. Our method fills this gap by leveraging DUSt3R [31] for pose-free reconstruction, enabling both self-supervised and zero-shot detection.

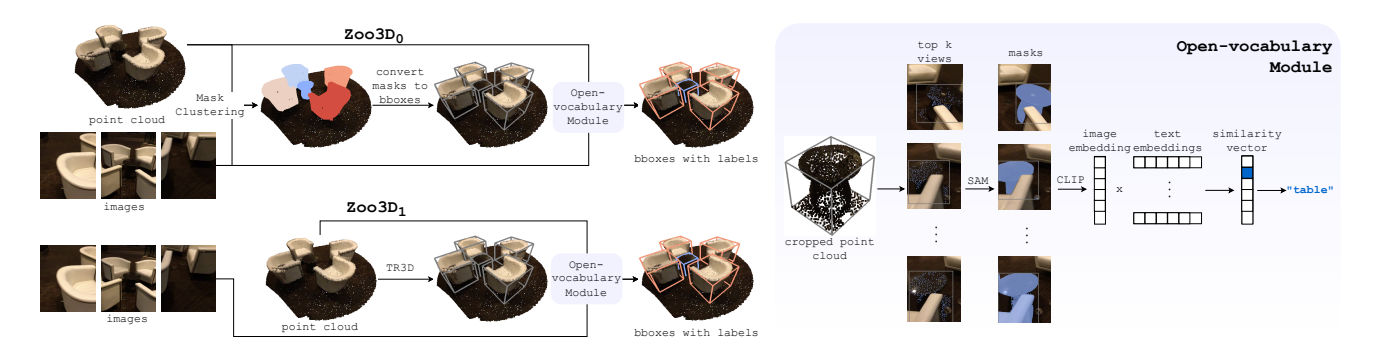


Figure 2. Inference pipeline of Zoo3D given point cloud inputs. Zoo3D<sub>0</sub> leverages MaskClustering to predict class-agnostic 3D bounding boxes from a point cloud and images (top-left), while Zoo3D<sub>1</sub> infers 3D bounding boxes from point clouds with TR3D (bottom-left). Both Zoo3D<sub>0</sub> and Zoo3D<sub>1</sub> assign semantic labels to 3D bounding boxes with the same Open-vocabulary Module (right). Given images, a full point cloud, and a 3D bounding box of an object, it crops the point cloud using the 3D bounding box, selects top k views based on the visibility, and projects visible points of the object onto these views. Object masks are obtained with SAM, CLIP embeddings are aggregated across views, and the text label with the most similar embedding is assigned.

# 3. Open-vocabulary 3D Object Detection from Point Clouds

Our work targets open-vocabulary 3D object detection, where the model must localize and recognize arbitrary objects. The open-vocabulary setting implies the absence of ground-truth 3D bounding box annotations. Recent annotation-free approaches exploit alternative supervision such as point clouds, RGB images, and camera trajectories, often leveraging powerful foundation models (e.g., CLIP, SAM) to align visual and text modalities. While these methods reduce dependence on manual labels, they still require access to training data.

To the best of our knowledge, no existing method can perform open-vocabulary 3D object detection entirely in a training-free manner, without using any form of training data. We are the first to address this challenge in a zero-shot setting. Below, we formalize the problem in Sec. 3.1, and present our zero-shot framework,  $Zoo3D_0$ , in Sec. 3.2. Furthermore, we extend these ideas to a self-supervised variant,  $Zoo3D_1$ , in Sec. 3.3, which leverages unlabeled data to enhance detection performance.

#### 3.1. Problem Formulation

3D object detection implies estimating 3D bounding boxes of individual objects, given inputs in a form of a point cloud, images, depths, camera poses, camera intrinsics, or any combination of them. Particularly, Zoo3D model awaits a point cloud  $\mathcal{P}=\{p_i\}_{i=1}^N\subset\mathbb{R}^3,$  where each point  $p_i=(x_i,y_i,z_i)$  is described with its coordinates in the 3D space, color images  $\mathcal{I}=\{I_1,I_2,\ldots,I_T\},$  their corresponding depths  $\mathcal{D}=\{D_1,D_2,\ldots,D_T\},$  camera extrinsics  $\mathcal{R}=\{R_1,R_2,\ldots,R_T\}$  and intrinsic K. 3D objects are parameterized as  $\mathcal{O}=\{(b_g,l_g)\}_{g=1}^G,$  where  $l_g\in\{1,\ldots,L\}$  denotes object open-vocabulary labels and  $b_g$  stands for the

spatial parameters of a 3D bounding box.  $b_g = (c_g, s_g)$ , where  $c_g \in \mathbb{R}^3$  is the center of a 3D bounding box and  $s_g \in \mathbb{R}^3_+$  are sizes along the x, y, z-axes.

# 3.2. Zero-shot 3D Object Detection: Zoo3D<sub>0</sub>

In Zoo3D, we decompose open-vocabulary 3D object detection into class-agnostic 3D object detection and open-vocabulary label assignment. First, we predict class-agnostic 3D bounding boxes  $\{b_g\}_{g=1}^G$ . Then, each box gets assigned with a semantic label  $l_g$  in our novel open-vocabulary module.

Class-agnostic 3D object detection is built upon zeroshot 3D instance segmentation method, namely, state-ofthe-art MaskClustering [33]. The original approach operates on color images  $\mathcal{I}$ , depths  $\mathcal{D}$ , camera extrinsics  $\mathcal{R}$  and a reconstructed point cloud  $\mathcal{P}$  and returns points with instance labels. We extend this approach so that it outputs 3D bounding boxes, thereby serving as a class-agnostic 3D object detection method.

The pipeline is organized as follows. First, a classagnostic mask predictor produces 2D masks  $\{m_{t,i}\}$  for each frame. These masks are used as nodes in a mask graph, with edges connecting masks belonging to the same instance. This graph is built iteratively by adding edges between highly conformed masks. For mask  $m_{t',i}$  in the frame t' and mask  $m_{t'',j}$  in the frame t'', we calculate view consensus rate  $\operatorname{cr}(m_{t',i},m_{t'',j})$  as a measure of conformity. To this end, we find all observer frames  $F_o$  where both masks  $m_{t',i}$  and  $m_{t'',j}$  are visible. Among those views, we find supporter frames  $F_s \in F_o$ : a view t is a supporter if it contains a mask  $m_{t,k}$  whose point cloud  $P_{t,k}$  includes the visible portions from point clouds  $P_{t',i}^t, P_{t'',j}^t$  of both  $m_{t',i}$  and

 $m_{t'',j}$ . The consensus rate is the supporter-observer ratio:

$$\mathrm{cr}(m_{t',i},m_{t'',j}) = \frac{|\{t \in V \mid \exists k, P_{t',i}^t, P_{t'',j}^t \sqsubset P_{t,k}\}|}{|F_o|}.$$

An edge is created if  $\operatorname{cr}(m_{t',i}, m_{t'',j}) \geq \tau_{rate} = 0.9$ . For each mask  $m_{t',i}$ , denoting the set of all masks that contain it across views as  $M(m_{t',i})$ , and its set of visible frames  $F(m_{t',i})$ , the consensus rate can be rewritten as:

$$\operatorname{cr}(m_{t',i}, m_{t'',j}) = \frac{|M(m_{t',i}) \cap M(m_{t'',j})|}{|F(m_{t',i}) \cap F(m_{t'',j})|}.$$

Masks are merged iteratively. In each iteration k, we remove edges with less than  $n_k$  observers, and merge connected components into new nodes. The final 3D instance masks are turned into 3D bounding boxes. Since we consider only axis-aligned boxes without rotation, the task boils down to getting minimum and maximum coordinates of 3D points belonging to each mask.

**Open-vocabulary module** assigns class-agnostic 3D bounding boxes with open-vocabulary semantic labels to each bounding box. First, we crop a point cloud  $\mathcal{P}$  with a bounding box  $b_a$ :

$$\mathcal{P}_g = \{ p_i \in \mathcal{P} \mid c_g - \frac{s_g}{2} \le p_i \le c_g + \frac{s_g}{2} \}.$$

Using the camera intrinsic and extrinsics, we project the 3D points from  $\mathcal{P}_g$  onto the 2D images. The projection of a 3D point  $p_i$  onto frame t is given by:

$$u_{t,i} = \pi(KR_t[x_i, y_i, z_i, 1]^T).$$

where  $\pi$  is the perspective projection operation  $\pi([x,y,w]^T)=[\frac{x}{w},\frac{y}{w}].$ 

Next, we backproject points and filter out significantly displaced points to avoid occlusions:

$$a_{t,i} = (K^{-1}[u_{t,i}, 1]^T) \cdot D_t(u_{t,i}),$$

$$\mathcal{U}_q^t = \left\{ u_{t,i} \mid ||p_i - (R_t^{-1}[a_{t,i}, 1]^T)_{x,y,z}|| < \tau_{\text{occ}} \right\}.$$

where  $\mathcal{U}_g^t$  – filtered points of bounding box  $b_g$  projected on image  $I_t$ ,  $\tau_{\rm occ}$  is the occlusion threshold.

We then select the top five images with the largest number of projected points. Since the predicted bounding boxes have some inherent error, the projection of the mask  $\mathcal{U}_g^t$  may not align perfectly with the object in the image. To solve this problem, we frame the projected points with a 2D bounding box using a min/max operation:

$$\mathbf{bb}_{2d} = [\min(\mathcal{U}_{g,x}^t), \min(\mathcal{U}_{g,y}^t), \max(\mathcal{U}_{g,x}^t), \max(\mathcal{U}_{g,y}^t)].$$

This 2D bounding box serves as an initial prompt for SAM, which returns a refined segmentation mask. This mask is

then processed at three different scales, as in MaskClustering, and fed into CLIP to obtain a feature vector. Finally, the average feature vector across five images and three scales is used to compute the cosine similarity with the feature vectors of the class names, thus yielding the labels and confidences for an arbitrary set of classes.

# 3.3. Self-supervised 3D Object Detection: Zoo3D<sub>1</sub>

Our training-free solution already sets a state-of-the-art even compared with self-supervised methods. Next, we explore how the accuracy can be pushed even higher utilizing our zero-shot model as a basis. Specifically, we run  $Zoo3D_0$  to generate class-agnostic 3D bounding boxes for training scenes, and train a class-agnostic 3D object detection model on the obtained labeled dataset in a self-supervised mode.

Class-agnostic 3D object detection model We build upon 3D object detection TR3D [25] and introduce modifications to adapt it to open vocabulary scenario. input point clouds are voxelized into 2 cm voxels and processed with a 3D sparse ResNet [23] that transforms the voxel space into 8 cm, 16 cm, 32 cm, and 64 cm-sized spatial grids. Neck aggregates 3D voxel features from four residual levels of the backbone. at levels of 64 cm and 32 cm, generative convolutional layers are added in order to prevent information loss and preserve the visibility field.

The detection head consists of two stacked linear layers. TR3D splits objects of interest into "large" and "small" based on their category, and predicts objects of each size with a dedicated head: "large" objects are predicted at 32-cm level, while "small" objects are inferred at 16-cm level. since we operate in open vocabulary mode, we cannot predefine any category-based routing. Accordingly, we use only the 16 cm-level.

Besides, we do not need to predict the object category but just estimate probability of object's presence, we omit classification-related part of the original model. In our class-agnostic model, the head returns a set of 3D locations  $\hat{\mathcal{V}} = \{\hat{v}_j\}_{j=1}^J$ . for each location  $\hat{v}_j \in \hat{\mathcal{V}}$ , it returns an objectness logit  $\tilde{z}_j \in \mathbb{R}^1$ , an offset of the center of an object  $\Delta c_j \in \mathbb{R}^3$ , and log-sizes of its 3D bounding box  $\tilde{s}_j \in \mathbb{R}^3$ . The canonical representation of the predicted 3D bounding box is derived as  $c_j = \hat{v}_j + \Delta c_j$ ,  $s_j = \exp(\tilde{s}_j) \in \mathbb{R}^3_+$ , while the resulting class probabilities are calculated as  $p_j = \sigma(\tilde{z}_j)$ .

**Training procedure** The assigner is used to couple the 3D locations  $\hat{v}_j$  with the ground truth objects  $\mathcal{O}_{gl}$ . Each ground truth object is assigned to the six nearest locations to its center. The loss function is bi-component, with components corresponding to head outputs. Namely, objectness prediction in the 3D object detection head is guided with a

Mathad	Seen during training				
Method	Scenes	3D bounding boxes			
Zoo3D <sub>0</sub>	Х	Х			
$Zoo3D_1$	✓	generated w/ Zoo3D <sub>0</sub>			
$Zoo3D_2$	✓	generated w/ Zoo3D <sub>1</sub>			

Table 1. Data used for training Zoo3D models.



Figure 3. Three operation modes of Zoo3D: with images with corresponding camera poses and point clouds as inputs (a), posed images (b) and unposed images (c). Ground truth input modalities are marked blue. In two latter scenarios, missing modalities are derived using DUSt3R.

focal loss  $\mathcal{L}_{focal}$  and regression of 3D bounding box parameters is being trained with DIoU loss  $\mathcal{L}_{DIoU}$ :

$$\mathcal{L} = \mathcal{L}_{focal} + \mathcal{L}_{DIoU}$$
.

Iterative training  $Zoo3D_1$  is trained with class-agnostic 3D bounding boxes generated by  $Zoo3D_0$ . Experiments show that the first iteration of this procedure improves the quality. Guided by this observation, we perform the second iteration of the procedure. Specifically, we re-generate annotations now using  $Zoo3D_1$ , and reproduce the training procedure with the same model and the same hyperparameters as  $Zoo3D_1$ , but with updated annotations. this iteration of labeling and training gives  $Zoo3D_2$ . in Tab. 1, we overview data involved in the training process of  $Zoo3D_0$ ,  $Zoo3D_1$ ,  $Zoo3D_2$ .

# **4.** Open-vocabulary 3D Object Detection from Multi-view Images

### 4.1. Posed Images

In the pose-aware scenario, our method accepts a set of images  $\mathcal{I}$  along with camera extrinsics  $\mathcal{R}$  and camera intrinsic K. In real applications, camera poses may be obtained from IMU or integrated tracking software.

Since we are able to handle point clouds, all we need is to transform images into a point cloud. For this purpose, we employ DUSt3R [31]. It can either infer camera poses or take them as auxiliary inputs, making it a universal solution for both pose-aware and pose-agnostic inference. Last but not least, opting for DUSt3R allows keeping the whole pipeline zero-shot and prevent data leakage, since contrary to some latest methods [30] it was not trained on ScanNet.

For input images, DUSt3R returns dense depth maps, that are fused into a TSDF volume using ground truth camera poses. The final step of this pipeline is the point cloud extraction, and the task is thus reduced to the point cloud-based 3D object detection.

## 4.2. Unposed Images

In the third scenario, our model is given images  $\mathcal{I}$  without known camera intrinsic K and extrinsics  $\mathcal{R}$ , which is the typical scenario for smartphone applications or capturing done with consumer cameras.

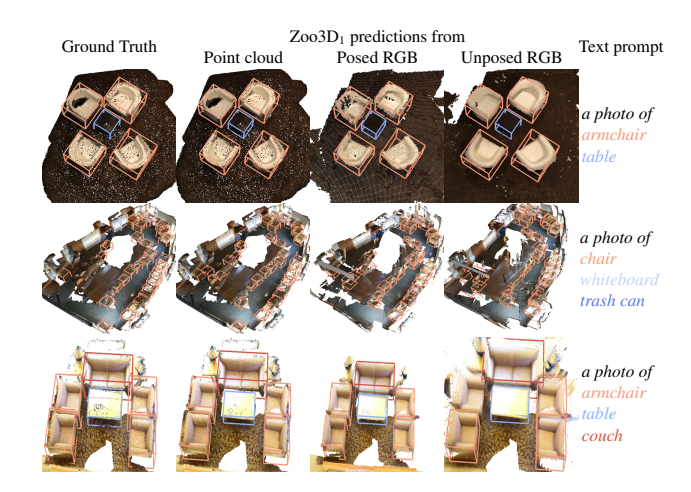


Figure 4. Qualitative results of Zoo3D<sub>1</sub> on ScanNet200.

DUSt3R shines in this most challenging setting, inferring depth maps and camera poses within a single end-to-end framework. Same as in the previous case, the predicted depth maps are fused, and the point cloud is extracted from the TSDF volume.

#### 5. Experiments

**Datasets** ScanNet [4] is a widely used dataset containing 1201 training and 312 validation scans. Following [17], we estimate axis-aligned 3D bounding boxes from semantic per-point labels. We report results obtained in four benchmarks based on ScanNet: ScanNet10 [13], ScanNet20 [14], ScanNet60 [32] and ScanNet200 [22], containing 10, 20, 60, and 200 classes, respectively. In the ScanNet60 benchmark, models are trained with ground truth 3D bounding boxes of objects from the first 10 classes in a classagnostic regime, and evaluated on all 60 classes in the open-vocabulary mode. In other benchmarks, annotated 3D bounding boxes are not seen during training. For all ScanNet-based benchmarks, we don't use ground truth 3D bounding boxes and report mean average precision (mAP) under IoU thresholds of 0.25 and 0.5.

ARKitScenes [2] is an RGB-D dataset of 4493 training scans and 549 validation scans. These scans contain RGB-D frames along with 3D object bounding box annotations of

Method	Venue	Zero-	Scanl	Net20	Scanl	Net60	ScanNet200	
Method	venue	shot	$mAP_{25}$	$mAP_{50}$	$mAP_{25}$	$mAP_{50}$	$mAP_{25}$	$mAP_{50}$
Point cloud + posed images								
Det-PointCLIPv2 <sup>†</sup> [46]	ICCV'23	X	-	-	0.2	-	-	-
3D-CLIP <sup>†</sup> [19]	ICML'21	X	-	-	3.9	-	-	-
OV-3DET [14]	CVPR'23	X	18.0	-	-	-	-	-
CoDa <sup>†</sup> [3]	NIPS'23	X	19.3	-	9.0	-	-	-
INHA <sup>†</sup> [10]	ECCV'24	X	-	-	10.7	-	-	-
GLIS [16]	ECCV'24	X	20.8	-	-	-	-	-
ImOV3D [34]	NIPS'24	X	21.5	-	-	-	-	-
OV-Uni3DETR <sup>†</sup> [32]	ECCV'24	X	25.3	-	19.4	-	-	-
$Zoo3D_0$	-	✓	34.7	23.9	27.1	18.7	21.1	14.1
$Zoo3D_1$	-	X	37.2	26.3	32.0	20.8	23.5	15.2
Posed images								
OV-Uni3DETR <sup>†</sup> [32]	ECCV'24	X	-	-	11.2	-	-	-
SAM3D [35] $\rightarrow$ OpenM3D [7]	ICCV'25	X	16.7	5.2	-	-	3.9	-
OV-3DET [14] $\rightarrow$ OpenM3D [7]	ICCV'25	X	17.7	2.9	-	-	3.1	-
OpenM3D [7]	ICCV'25	X	19.8	7.3	-	-	4.2	-
DUSt3R [31] $\rightarrow$ Zoo3D <sub>0</sub>	-	✓	30.5	17.3	22.0	10.4	14.3	6.2
$DUSt3R [31] \rightarrow Zoo3D_1$	-	X	32.8	15.5	23.9	10.8	16.5	6.3
Unposed images								
DUSt3R [31] $\rightarrow$ Zoo3D <sub>0</sub>	-	✓	24.2	8.8	13.3	4.1	8.3	2.9
DUSt3R [31] $\rightarrow$ Zoo3D <sub>1</sub>	=	Х	27.9	10.4	15.3	5.6	10.7	3.8

Table 2. Results of open-vocabulary 3D object detection on the ScanNet dataset across three benchmarks (with 20, 60, and 200 classes), and three input modalities (points cloud, posed and unposed multi-view images). Methods with  $^{\dagger}$  utilize 3D bounding box annotations during training. Our Zoo3D significantly outperforms prior work even in the zero-shot setting. Self-supervised Zoo3D<sub>1</sub> using only unposed images performs on par with point cloud- based methods.

17 categories. We use ARKitScenes for class-agnostic evaluation, following the protocol proposed by OpenM3D [7], and report standard precision and recall.

Implementation details Zero-shot  $Zoo3D_0$  is training-free and uses the same hyperparameters as the original MaskClustering [33] during the inference. Self-supervised  $Zoo3D_1$  inherits the training hyperparameters of TR3D [25]. To control the size of input scenes, we sample a maximum of 100,000 points per scene during both training and inference. During inference, candidate detections are filtered using NMS with an IoU threshold of 0.5. Architecture-wise, we modify TR3D as described in Sec. 3.3, keeping the rest of architecture the same as in the original TR3D. Our open-vocabulary module uses CLIP ViT-H/14 [19] and SAM 2.1 (Hiera-L) [20]. For each scene, we sample 45 images uniformly. Images are resized into  $480 \times 640$  in all experiments.

#### 5.1. Comparison with Prior Work

**Open-vocabulary 3D object detection from point clouds**We benchmark the proposed approach in the most common

scenario with ground truth point clouds as inputs and report scores on multiple benchmark on ScanNet with 10, 20, 60, and 200 classes. As reported in Tab. 2, our method demonstrates significant performance gains w.r.t. prior state-of-the-art open-vocabulary 3D object detection approaches (+11.9 mAP $_{25}$  on ScanNet20, +12.6 mAP $_{25}$  on ScanNet60 w.r.t. OV-Uni3DETR). Overall, with consistent improvement over all existing methods, Zoo3D sets a new state-of-the-art in 3D open-vocabulary object detection. According to Tab. 3 presenting the results on the ScanNet10 benchmark, we achieve competitive results even in a zero-shot setting, while our self-supervised model outperforms the closest competitor, OV-Uni3Detr, by +10.4 mAP25.

**Open-vocabulary 3D object detection from posed images** is a more challenging task gaining attention recently, so in this competitive track we test against approaches leveraging state-of-the-art techniques. Still, Zoo3D shines, with +10.1 mAP<sub>25</sub> ScanNet200 w.r.t. OpenM3D and +12.7 mAP<sub>25</sub> ScanNet60 w.r.t. OV-Uni3DETR achieved in self-supervised mode. Surprisingly, even without access to ground truth point clouds, Zoo3D outperforms point cloud-

Method	mAP <sub>25</sub>	mAP <sub>50</sub>
OV-3DETIC <sup>†</sup> [13]	12.7	-
FM-OV3D [40]	17.0	-
FM-OV3D <sup>†</sup> [40]	21.5	-
Object2Scene <sup>†</sup> [44]	24.6	-
INHA <sup>†</sup> [10]	30.1	-
GLIS [16]	30.9	-
OV-Uni3DETR <sup>†</sup> [32]	34.1	-
$Zoo3D_0$	42.1	28.7
$Zoo3D_1$	44.5	31.5

Table 3. Results of open-vocabulary 3D object detection from point clouds on the ScanNet10 benchmark. Methods with † utilize 3D bounding box annotations during training.

based approaches in both zero-shot and self-supervised scenario. This is a strong evidence that with a thoughtfully designed pipeline, we can beat state-of-the-art without training and having less data on inference.

Open-vocabulary 3D object detection from unposed images In the third track, there are no predecessors reporting 3D open-vocabulary object detection results. Respectively, we also obtain reference numbers with a combination of DUSt3R  $\rightarrow$  Zoo3D0 and DUSt3R  $\rightarrow$  Zoo3D1. As could be expected, DUSt3R  $\rightarrow$  Zoo3D1 outperforms DUSt3R  $\rightarrow$  Zoo3D0. What is more exciting is that the performance of our self-supervised Zoo3D1 is close to the one of OV-Uni3DETR using point clouds. In other words, being exposed to the same training data, but with neither point clouds nor even camera poses on inference, our method can deliver competitive accuracy to point cloud-based solutions.

Class-agnostic 3D object detection is less studied, with existing methods only using posed images as inputs and reporting quality on ScanNet200. Still, we report metrics across all three input modalities and three benchmarks to establish the baseline for future research. Our zero-shot model is inferior to OpenM3D, while self-supervised Zoo3D<sub>1</sub> surpasses it by a large margin, achieving +9 mAP<sub>25</sub>.

### **5.2. Ablation Experiments**

Class-agnostic 3D object detection (OpenM3D protocol) implies calculating precision and recall for class-agnostic 3D bounding boxes on ScanNet200 and ARK-itScenes. This alternative evaluation protocol is more coherent with how those boxes are used in our pipeline: we omit low-confidence boxes and only pass reliable detections to the open-vocabulary module, so the predictions are turned binary rather than probabilistic. As seen from Tab. 5, Zoo3D<sub>0</sub> only slightly outperforms previous state-of-the-art in precision and recall calculated at the threshold of 0.25.

When limiting the evaluation scope to more accurate detections with a threshold of 0.5, the superiority of Zoo3D<sub>0</sub> becomes more prominent, i.e., metrics on ARKitScenes double, while the ScanNet scores rise by approx 50%.

**Inference time** Up to a certain degree, the superior quality of our approach should be attributed to the significantly longer processing time. In Tab. 6, we report inference time of Zoo3D<sub>0</sub> and Zoo3D<sub>1</sub> in comparison to the OpenM3D, an efficient single-stage feed-forward method. OpenM3D does not require a separate open-vocabulary module with CLIP, achieving impressive performance that comes at the cost of accuracy. Still, the most time-expensive component of our pipeline is point cloud reconstruction, which is performed with DUSt3R. The latency of Zoo3D<sub>0</sub> and Zoo3D<sub>1</sub> also differs due to distinct class-agnostic 3D object detection strategies applied. While Zoo3D<sub>0</sub> builds a mask graph, which can be slow, the self-supervised method uses a lightweight sparse-convolutional model. However, mask clustering procedure assigns instance labels unambiguously by design, while detection model produces numerous duplicates. Respectively, more detections should be processed at the openvocabulary stage, leading to 7x increase of inference time.

Number of images per scene In Tab. 7, we ablate  $Zoo3D_0$  against varying number of images per scenes. The model hits the peak with 45 frames, and performs on par with OpenM3D and OV-Uni3DETR using 20 frames. On ScanNet200,  $Zoo3D_0$  outperforms OpenM3D with as few as 15 images.

**DUSt3R vs DROID-SLAM** As an alternative to DUSt3R for point cloud reconstruction, we use DROID-SLAM, a well-known reconstruction method based on entirely different working principles. According to Tab. 8, quality drops dramatically when switching to DROID-SLAM: apparently, DROID-SLAM fails to produce reconstructions of quality that allows localizing and recognizing 3D objects reliably.

**Iterative training** is ablated in Tab. 9.  $Zoo3D_2$  denotes the self-supervised model trained with annotations generated by  $Zoo3D_1$ . Evidently, the iterative training process results in an improvement between steps 0 and 1, and between 1 and 2. However, performance gradually saturates, and by the third iteration, the metrics cease to improve.

**Open-vocabulary module** consists of three components, namely, occlusion filter, SAM-based mask refinement and multi-scale processing. We evaluate the contribution of each component by switching if off and measuring quality degradation. Instead of SAM mask refinement, we simply

Method	Zero-shot	Scan	Net20	Scan	Net60	ScanN	let200
Method	Zeio-silot	$mAP_{25}$	$mAP_{50}$	$mAP_{25}$	$mAP_{50}$	$mAP_{25}$	$mAP_{50}$
Point cloud + posed images							
$Zoo3D_0$	✓	36.0	21.9	29.6	16.5	32.1	17.6
$Zoo3D_1$	X	46.1	30.9	48.5	29.6	51.0	31.0
Posed images							
OV-3DET [14] $\rightarrow$ OpenM3D [7]	×	-	-	-	-	19.5	-
SAM3D [35] $\rightarrow$ OpenM3D [7]	×	-	-	-	-	23.8	-
OpenM3D [7]	×	-	-	-	-	26.9	-
DUSt3R [31] $\rightarrow$ Zoo3D <sub>0</sub>	✓	31.3	12.4	22.0	7.3	22.4	6.8
$DUSt3R~[31] \rightarrow Zoo3D_1$	X	40.1	18.9	35.0	14.0	36.1	13.9
Unposed images							
DUSt3R [31] $\rightarrow$ Zoo3D <sub>0</sub>	$\checkmark$	16.4	2.5	10.1	1.5	10.3	1.5
DUSt3R [31] $\rightarrow$ Zoo3D <sub>1</sub>	Х	22.7	5.7	18.3	4.0	19.0	3.9

Table 4. Results of class-agnostic 3D object detection on the ScanNet dataset across three benchmarks (with 20, 60, and 200 classes), and three input modalities (points cloud, posed and unposed multi-view images).

Method		ScanN	Vet200			ARKit	Scene	s
	P <sub>25</sub>	R <sub>25</sub>	P <sub>50</sub>	R <sub>50</sub>	P <sub>25</sub>	R <sub>25</sub>	P <sub>50</sub>	R <sub>50</sub>
OV-3DET [14]	11.6	21.3	4.4	8.0	3.7	32.4	0.9	7.9
SAM3D [35]	14.5	57.7	9.0	36.1	6.0	43.8	1.5	10.9
OpenM3D [7]	32.0	58.3	18.1	33.0	5.9	51.9	1.6	13.7
$Zoo3D_0$	35.9	<b>58.7</b>	27.9	45.6	8.4	52.0	4.3	28.2

Table 5. Results of class-agnostic 3D object detection on Scan-Net200 and ARKitScenes, OpenM3D evaluation protocol. P- precision, R- recall.

Method	Reconst.	Detect.	Open-vocab.
OpenM3D [7]	_	0.3	0.01
DUSt3R [31] $\rightarrow$ Zoo3D <sub>0</sub>	294.3	56.3	12.6
$DUSt3R~[\textbf{31}] \rightarrow Zoo3D_1$	294.3	0.04	84.0

Table 6. Inference time (sec) of 3D object detection from posed images on ScanNet200, component-wise: reconstruction (DUSt3R), class-agnostic 3D object detection, and open-vocabulary module.

# Images	Pos	sed	Unp	osed
# Images	$mAP_{25}$	$mAP_{50}$	$mAP_{25}$	$mAP_{50}$
15	9.6	3.9	5.8	1.9
25	12.5	5.2	7.1	2.6
35	14.0	5.7	8.1	2.7
45	14.3	6.2	8.3	2.9

Table 7. Results of open-vocabulary 3D object detection from posed and unposed images on ScanNet200 with varying number of images.

Method	mAP <sub>25</sub>	mAP <sub>50</sub>
DROID-SLAM [28] $\rightarrow$ Zoo3D <sub>1</sub>	2.4	0.6
DUSt3R [31] $\rightarrow$ Zoo3D <sub>1</sub>	19.0	3.9

Table 8. Results of self-supervised method from unposed images in class-agnostic mode on ScanNet200 with different pose estimation methods.

Method	mAP <sub>25</sub>	mAP <sub>50</sub>
$\begin{array}{c} \text{DUSt3R [31]} \rightarrow \text{Zoo3D}_0 \\ \text{DUSt3R [31]} \rightarrow \text{Zoo3D}_1 \\ \text{DUSt3R [31]} \rightarrow \text{Zoo3D}_2 \end{array}$	22.4 36.1 <b>37.6</b>	6.8 13.9 <b>14.8</b>

Table 9. Results of class-agnostic 3D object detection from posed images on ScanNet200 with iterative training.

Module	mAP <sub>25</sub>	mAP <sub>50</sub>
base	14.7	5.7
+ occlusion filter	14.8	5.7
+ SAM mask refinement	15.4	5.7
+ multi-scale	16.5	6.3

Table 10. Results of open-vocabulary 3D object detection from posed images on ScanNet200, with different configurations of the open-vocabulary module.

project all the object's points onto the image and approximate mask with a bounding-box tightly enclosing the projected points. As can be observed in Tab. 10, multi-scale processing improves  $mAP_{50}$ , while SAM mask refinement contributes to  $mAP_{25}$ .

#### 6. Conclusion

We proposed a first-in-class zero-shot  $Zoo3D_0$  and a self-supervised  $Zoo3D_1$  open-vocabulary 3D object detection methods. Besides, we adapted Zoo3D to work directly with posed and even unposed images, so that point clouds are not required. Across multiple benchmarks, both  $Zoo3D_0$  and  $Zoo3D_1$  achieve state-of-the-art results in open-vocabulary 3D detection. As a possible future research direction, we consider speeding up the pipeline with elaborate procedures of harvesting spatial information from 2D foundation models: a faster reconstruction method, a better segmentation model, a more efficient open-vocabulary label assignment, and extensive use of large language models.

In Appendix, we provide additional quantitative scores, including evaluation results on ScanNet++ [38] and ARK-itScenes [2], in Sec. A, report results of ablation experiments in Sec. B, and show more visualizations in Sec. C.

### A. Quantitative Results

**ScanNet++** As can be seen from Tab. 11,  $Zoo3D_0$  sets state-of-the-art in ScanNet++ [38] even compared with fully-supervised methods. Despite not being exposed to any annotations or even training scenes, it outperforms models that utilize both scans and labeled 3D bounding boxes during the training.

**ScanNet60** results are reported in Tab. 12. For objects of *base* categories, Zoo3D falls beyond training-based competitors, which could be expected, since neither of our methods has access to ground truth 3D bounding boxes. For *novel* objects not seen during training, Zoo3D scores first in the leaderboard.

**3D segmentation baselines** Open-vocabulary 3D object detection metrics on ScanNet are listed in Tab. 13. To establish baselines, we adapt state-of-the-art 3D instance segmentation approaches by simply enclosing each predicted mask with a 3D bounding box. Obviously, while Zoo3D<sub>0</sub> is built upon MaskClustering, our open-vocabulary assignment strategy is way more effective compared to the one used in the original MaskClustering.

Method	mAP <sub>25</sub>	mAP <sub>50</sub>
TR3D <sup>†</sup> [25]	26.2	14.5
UniDet3D <sup>†</sup> [11]	26.4	17.2
$Zoo3D_0$	26.5	18.3

Table 11. 3D object detection results from points clouds on Scan-Net++ dataset. † is for fully-supervised method utilized labeled 3D bounding boxes during training.

Method	Zero- shot	Novel	Base	All
Det-PointCLIPv2 <sup>†</sup> [46]	X	0.1	1.0	0.2
3D-CLIP <sup>†</sup> [19]	X	2.5	11.2	3.9
CoDA <sup>†</sup> [3]	X	6.5	21.6	9.0
INHA <sup>†</sup> [10]	X	7.8	25.1	10.7
OV-Uni3DETR <sup>†</sup> [32]	X	13.7	48.1	19.4
$Zoo3D_0$	✓	29.3	16.2	27.1
$Zoo3D_1$	X	33.6	24.4	32.0

Table 12. Results of open-vocabulary 3D object detection of *base*, *novel*, and *all* object categories on ScanNet60. Methods marked with † use ground truth 3D bounding boxes for objects of *base* classes.

Method	Venue	mAP <sub>25</sub>	mAP <sub>50</sub>
MaskClustering [33] OnlineAnySeg [27]	CVPR'24 CVPR'25	13.4 19.0	8.5 12.3
$Zoo3D_0$	-	21.1	14.1

Table 13. Comparison with zero-shot 3D instance segmentation methods on ScanNet200.

**ARKitScenes** was used to train DUSt3R, so we cannot use it in zero-shot experiments for fair comparison. In this series of experiments, DUSt3R is replaced with VGGT to preserve methodological purity. Since VGGT does not support camera poses as inputs natively, we only report quality in point cloud-based and unposed images-based tracks in Tab. 15.

**Per-category scores** on ScanNet20 are given in Tab. 14. Evidently, both our methods outperform the competitors by a large margin, with the most significant gains achieved for *chair* (+45.7 mAP $_{25}$  for Zoo3D $_{1}$  over previous state-of-theart), *sofa* (+20.9), *bookshelf* (+19.7), *refridgerator* (+43.1), *nightstand* (+44.0), *lamp* (+37.7). The average mAP $_{25}$  of Zoo3D $_{0}$  is 9.4 higher than of any existing approach, while Zoo3D $_{1}$  further expands the gap to 11.9 mAP $_{25}$ .

### **B.** Ablation Experiments

VGGT vs DUSt3R for point cloud reconstruction is evaluated in Tab. 16. Evidently, VGGT surpasses DUSt3R by a large margin, which can be expected, since VGGT was trained on ScanNet. Unfortunately, this also means that we cannot use it in the zero-shot setting; so despite the superior performance of VGGT, we employ DUSt3R as our primary method in our ScanNet-based experiments.

**Level assignment strategy** In Tab. 17, we ablate assigner parameters. In the class-agnostic mode, object classes re-

Methods	mAP <sub>25</sub>	toilet	bed	chair	sofa	dresser	table	cabinet	bookshelf	pillow	sink
OV-3DET [14]	18.0	57.3	42.3	27.1	31.5	8.2	14.2	3.0	5.6	23.0	31.6
CoDA [3]	19.3	68.1	44.1	28.7	44.6	3.4	20.2	5.3	0.1	28.0	45.3
OV-Uni3DETR [32]	25.3	86.1	50.5	28.1	31.5	18.2	24.0	6.6	12.2	29.6	54.6
$Zoo3D_0$	34.7	91.1	51.2	53.4	60.5	31.9	20.2	12.9	41.9	32.2	25.7
$Zoo3D_1$	37.2	78.4	54.4	74.4	65.5	33.6	19.1	14.1	32.3	46.1	27.3
		bathtub	refrigerator	desk	nightstand	counter	door	curtain	box	lamp	bag
OV-3DET [14]		56.3	11.0	19.7	0.8	0.3	9.6	10.5	3.8	2.1	2.7
CoDA [3]		50.5	6.6	12.4	15.2	0.7	8.0	0.0	2.9	0.5	2.0
OV-Uni3DETR [32]		63.7	14.4	30.5	2.9	1.0	1.0	19.9	12.7	5.6	13.5
$Zoo3D_0$		50.0	50.5	11.2	59.2	0.1	21.1	18.2	17.8	34.8	9.8
$Zoo3D_1$		64.6	57.5	10.7	58.8	0.2	27.4	8.0	20.0	43.3	9.1

Table 14. Per-class 3D object detection scores on the ScanNet20.

Method	Zero-shot shot	mAP <sub>25</sub>	mAP <sub>50</sub>
Point cloud + posed images			
$Zoo3D_0$	✓	24.4	11.0
$Zoo3D_1$	×	34.2	24.2
Unposed images			
VGGT [30] $\rightarrow$ Zoo3D <sub>0</sub>	✓	13.0	2.6
VGGT [30] $\rightarrow$ Zoo3D <sub>1</sub>	×	16.1	3.5

Table 15. Results of open-vocabulary 3D object detection from points clouds on ARKitScenes.

main unknown during the training, so we cannot apply the category-aware assignment scheme used in the original TR3D. Namely, we try assigning all objects to the 16 cm-level or 32 cm-level, or split the objects based on their size 50/50. The results demonstrate that assigning all objects to the 16-cm level yields the best performance.

Method	Trained on ScanNet	mAP <sub>25</sub>	mAP <sub>50</sub>
DUSt3R [31] $\rightarrow$ Zoo3D <sub>1</sub>	×	19.0	3.9
VGGT [30] $\rightarrow$ Zoo3D <sub>1</sub>		<b>28.2</b>	<b>6.4</b>

Table 16. Results of class-agnostic Zoo3D<sub>1</sub> from unposed images on ScanNet200 with different pose estimation methods.

Object assignment	$mAP_{25}$	$mAP_{50}$
all objects to 32-cm level	31.2	9.8
50/50	34.5	12.3
all objects to 16-cm level	36.1	13.9

Table 17. Results of class-agnostic  $Zoo3D_1$  from posed images on ScanNet200 with different assignment strategies.

Alignment strategy	$mAP_{25}$	$mAP_{50}$
first 2 poses	4.1	0.8
first depth + first pose	8.3	2.9

Table 18. Results of  $Zoo3D_0$  from unposed images on ScanNet200 with different alignment stratagies.

Alignment with g/t in image-based scenarios In Tab. 18, we report results obtained with different alignment strategies. Here, point clouds are reconstructed from images; still, ground truth annotations are needed for evaluation, since scans must be transformed into common coordinate space before computing the metrics. To estimate an affine transformation that aligns ground truth and predicted point clouds, we apply two strategies. In the first strategy, we use both ground truth and predicted depth and pose for the first frame. The predicted pose is aligned with the ground truth pose, giving the rotation and translation. The scale is estimated from a single ground-truth depth map as the median of per-pixel ratios of ground-truth to predicted depth. In the second strategy, we use ground truth and predicted camera poses of two first frames in a sequence. The first predicted pose is aligned with the first ground truth pose, giving the rotation and translation. The relative scale coefficient is derived as a ratio of distances between two camera poses in predicted and ground truth scans.

# C. Qualitative Results

Open-vocabulary 3D object detection results on Scan-Net200 are shown in Fig. 5, while results on ARKitScenes and Scan-Net++ are presented in Fig. 6. We visualize predictions from different input modalities to provide intuition of how the prediction accuracy depends on the amount of information passed to the model.

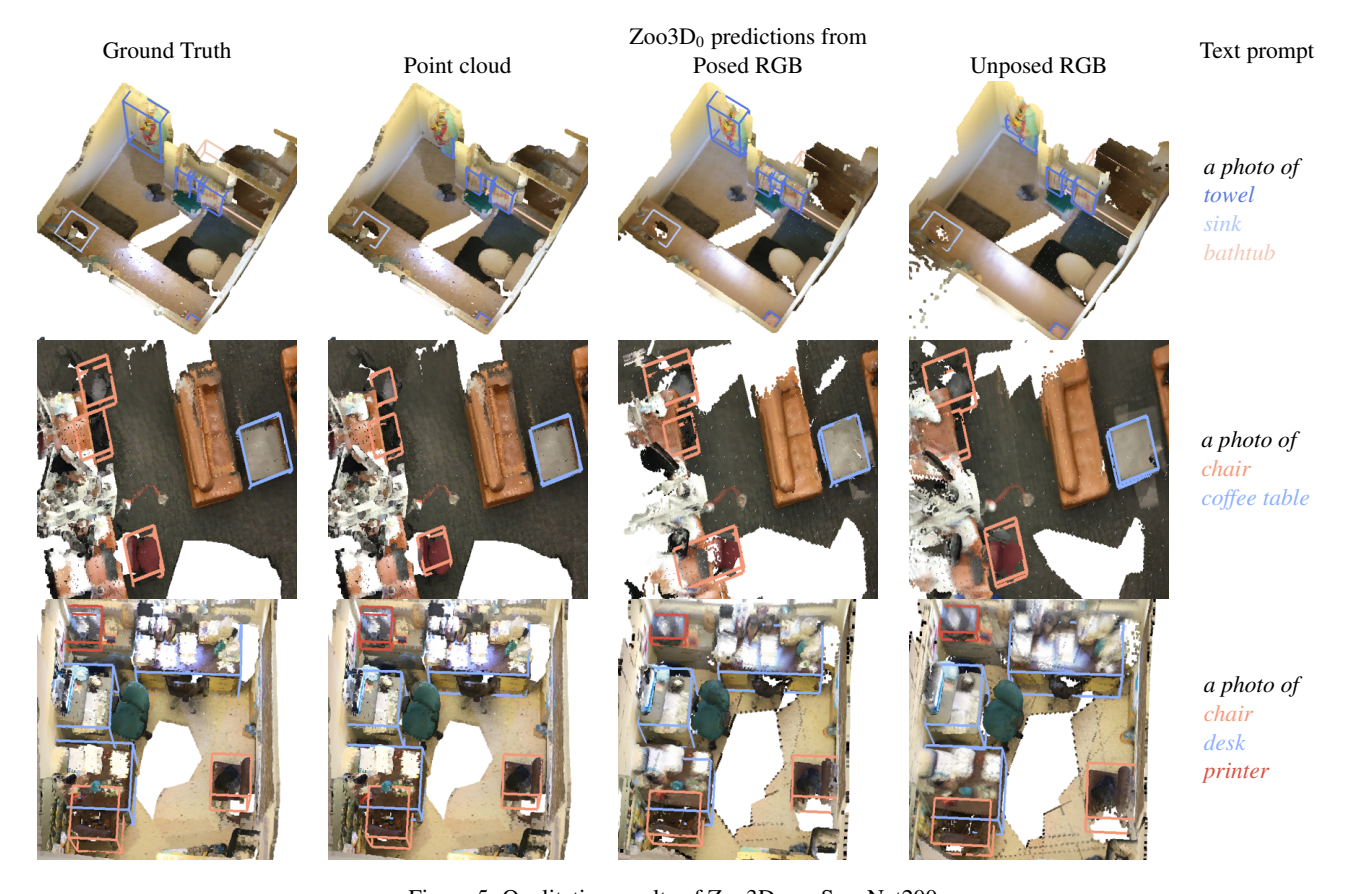


Figure 5. Qualitative results of  $Zoo3D_0$  on ScanNet200.

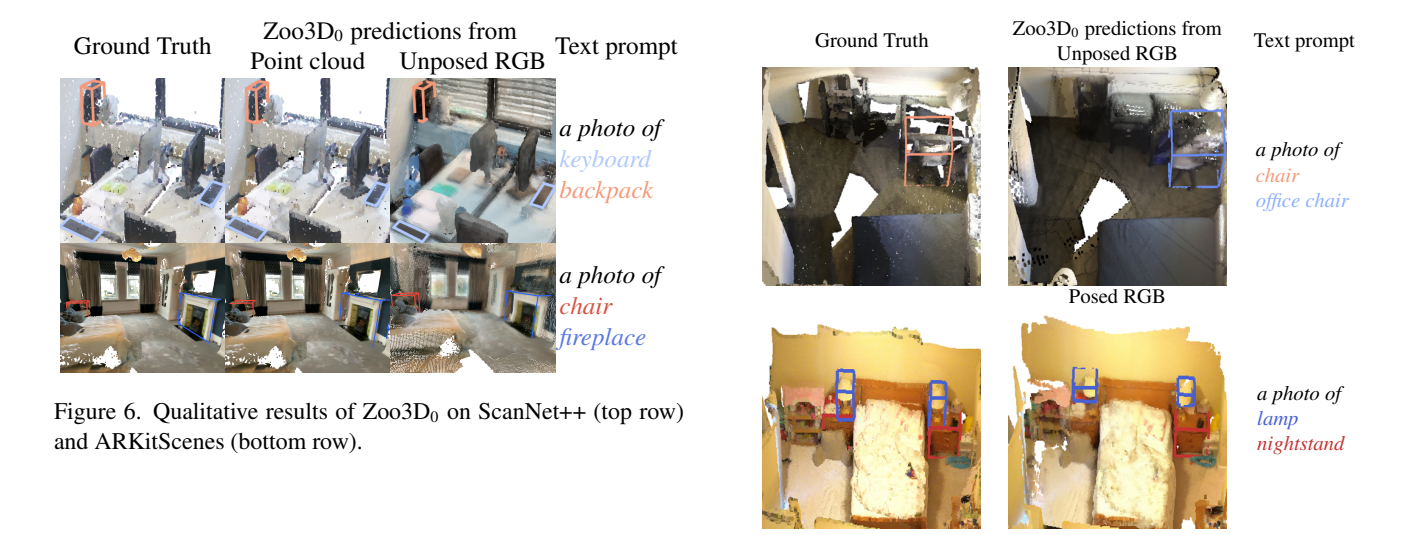


Figure 7. Failure cases of Zoo3D<sub>0</sub> on ScanNet200.

**Failure cases** are depicted in Fig. 7. Here we challenge our model in restrictive posed and unposed image-based scenarios. As metric values suggest, our model is prone to errors of various types: it can misclassify detected objects or even miss them in the scene entirely.

# References

[1] Shuai Bai, Keqin Chen, Xuejing Liu, Jialin Wang, Wenbin Ge, Sibo Song, Kai Dang, Peng Wang, Shijie Wang, Jun Tang, et al. Qwen2. 5-vl technical report. *arXiv preprint* 

- arXiv:2502.13923, 2025. 1
- [2] Gilad Baruch, Zhuoyuan Chen, Afshin Dehghan, Tal Dimry, Yuri Feigin, Peter Fu, Thomas Gebauer, Brandon Joffe, Daniel Kurz, Arik Schwartz, et al. Arkitscenes: A diverse real-world dataset for 3d indoor scene understanding using mobile rgb-d data. arXiv preprint arXiv:2111.08897, 2021. 5, 9
- [3] Yang Cao, Zeng Yihan, Hang Xu, and Dan Xu. Coda: Collaborative novel box discovery and cross-modal alignment for open-vocabulary 3d object detection. *Advances in Neural Information Processing Systems*, 36:71862–71873, 2023. 2, 6, 9, 10
- [4] Angela Dai, Angel X Chang, Manolis Savva, Maciej Halber, Thomas Funkhouser, and Matthias Nießner. Scannet: Richly-annotated 3d reconstructions of indoor scenes. In *Proceedings of the IEEE conference on computer vision and pattern recognition*, pages 5828–5839, 2017. 5
- [5] Zhiwen Fan, Jian Zhang, Renjie Li, Junge Zhang, Runjin Chen, Hezhen Hu, Kevin Wang, Huaizhi Qu, Dilin Wang, Zhicheng Yan, et al. Vlm-3r: Vision-language models augmented with instruction-aligned 3d reconstruction. arXiv preprint arXiv:2505.20279, 2025. 2
- [6] Dong Guo, Faming Wu, Feida Zhu, Fuxing Leng, Guang Shi, Haobin Chen, Haoqi Fan, Jian Wang, Jianyu Jiang, Jiawei Wang, et al. Seed1. 5-vl technical report. arXiv preprint arXiv:2505.07062, 2025. 1
- [7] Peng-Hao Hsu, Ke Zhang, Fu-En Wang, Tao Tu, Ming-Feng Li, Yu-Lun Liu, Albert YC Chen, Min Sun, and Cheng-Hao Kuo. Openm3d: Open vocabulary multi-view indoor 3d object detection without human annotations. In *Proceedings* of the IEEE/CVF International Conference on Computer Vision, pages 8688–8698, 2025. 1, 2, 6, 8
- [8] Chenxi Huang, Yuenan Hou, Weicai Ye, Di Huang, Xiaoshui Huang, Binbin Lin, and Deng Cai. Nerf-det++: Incorporating semantic cues and perspective-aware depth supervision for indoor multi-view 3d detection. *IEEE Transactions on Image Processing*, 2025. 2
- [9] Haifeng Huang, Yilun Chen, Zehan Wang, Rongjie Huang, Runsen Xu, Tai Wang, Luping Liu, Xize Cheng, Yang Zhao, Jiangmiao Pang, et al. Chat-scene: Bridging 3d scene and large language models with object identifiers. Advances in Neural Information Processing Systems, 37: 113991–114017, 2024.
- [10] Pengkun Jiao, Na Zhao, Jingjing Chen, and Yu-Gang Jiang. Unlocking textual and visual wisdom: Open-vocabulary 3d object detection enhanced by comprehensive guidance from text and image. In *European Conference on Computer Vi*sion, pages 376–392. Springer, 2024. 2, 6, 7, 9
- [11] Maksim Kolodiazhnyi, Anna Vorontsova, Matvey Skripkin, Danila Rukhovich, and Anton Konushin. Unidet3d: Multidataset indoor 3d object detection. In *Proceedings of the* AAAI Conference on Artificial Intelligence, pages 4365– 4373, 2025. 1, 2, 9
- [12] Shilong Liu, Zhaoyang Zeng, Tianhe Ren, Feng Li, Hao Zhang, Jie Yang, Qing Jiang, Chunyuan Li, Jianwei Yang, Hang Su, et al. Grounding dino: Marrying dino with grounded pre-training for open-set object detection. In *Euro*-

- pean conference on computer vision, pages 38–55. Springer, 2024. 1
- [13] Yuheng Lu, Chenfeng Xu, Xiaobao Wei, Xiaodong Xie, Masayoshi Tomizuka, Kurt Keutzer, and Shanghang Zhang. Open-vocabulary 3d detection via image-level class and debiased cross-modal contrastive learning. arXiv preprint arXiv:2207.01987, 2022. 2, 5, 7
- [14] Yuheng Lu, Chenfeng Xu, Xiaobao Wei, Xiaodong Xie, Masayoshi Tomizuka, Kurt Keutzer, and Shanghang Zhang. Open-vocabulary point-cloud object detection without 3d annotation. In *Proceedings of the IEEE/CVF conference on* computer vision and pattern recognition, pages 1190–1199, 2023. 1, 2, 5, 6, 8, 10
- [15] Yongsen Mao, Junhao Zhong, Chuan Fang, Jia Zheng, Rui Tang, Hao Zhu, Ping Tan, and Zihan Zhou. Spatiallm: Training large language models for structured indoor modeling. arXiv preprint arXiv:2506.07491, 2025. 1, 2
- [16] Xingyu Peng, Yan Bai, Chen Gao, Lirong Yang, Fei Xia, Beipeng Mu, Xiaofei Wang, and Si Liu. Global-local collaborative inference with llm for lidar-based open-vocabulary detection. In *European Conference on Computer Vision*, pages 367–384. Springer, 2024. 2, 6, 7
- [17] Charles R Qi, Or Litany, Kaiming He, and Leonidas J Guibas. Deep hough voting for 3d object detection in point clouds. In proceedings of the IEEE/CVF International Conference on Computer Vision, pages 9277–9286, 2019. 1, 5
- [18] Zhangyang Qi, Zhixiong Zhang, Ye Fang, Jiaqi Wang, and Hengshuang Zhao. Gpt4scene: Understand 3d scenes from videos with vision-language models. arXiv preprint arXiv:2501.01428, 2025. 1, 2
- [19] Alec Radford, Jong Wook Kim, Chris Hallacy, Aditya Ramesh, Gabriel Goh, Sandhini Agarwal, Girish Sastry, Amanda Askell, Pamela Mishkin, Jack Clark, et al. Learning transferable visual models from natural language supervision. In *International conference on machine learning*, pages 8748–8763. PmLR, 2021. 2, 6, 9
- [20] Nikhila Ravi, Valentin Gabeur, Yuan-Ting Hu, Ronghang Hu, Chaitanya Ryali, Tengyu Ma, Haitham Khedr, Roman Rädle, Chloe Rolland, Laura Gustafson, et al. Sam 2: Segment anything in images and videos. *arXiv preprint arXiv:2408.00714*, 2024. 2, 6
- [21] Tianhe Ren, Shilong Liu, Ailing Zeng, Jing Lin, Kunchang Li, He Cao, Jiayu Chen, Xinyu Huang, Yukang Chen, Feng Yan, et al. Grounded sam: Assembling open-world models for diverse visual tasks. *arXiv preprint arXiv:2401.14159*, 2024. 1
- [22] David Rozenberszki, Or Litany, and Angela Dai. Language-grounded indoor 3d semantic segmentation in the wild. In *European conference on computer vision*, pages 125–141. Springer, 2022. 5
- [23] Danila Rukhovich, Anna Vorontsova, and Anton Konushin. Fcaf3d: Fully convolutional anchor-free 3d object detection. In *European Conference on Computer Vision*, pages 477–493. Springer, 2022. 1, 2, 4
- [24] Danila Rukhovich, Anna Vorontsova, and Anton Konushin. Imvoxelnet: Image to voxels projection for monocular and multi-view general-purpose 3d object detection. In *Proceed*-

- ings of the IEEE/CVF winter conference on applications of computer vision, pages 2397–2406, 2022. 2
- [25] Danila Rukhovich, Anna Vorontsova, and Anton Konushin. Tr3d: Towards real-time indoor 3d object detection. In 2023 IEEE International Conference on Image Processing (ICIP), pages 281–285. IEEE, 2023. 1, 2, 4, 6, 9
- [26] Yichao Shen, Zigang Geng, Yuhui Yuan, Yutong Lin, Ze Liu, Chunyu Wang, Han Hu, Nanning Zheng, and Baining Guo. V-detr: Detr with vertex relative position encoding for 3d object detection. arXiv preprint arXiv:2308.04409, 2023. 1,
- [27] Yijie Tang, Jiazhao Zhang, Yuqing Lan, Yulan Guo, Dezun Dong, Chenyang Zhu, and Kai Xu. Onlineanyseg: Online zero-shot 3d segmentation by visual foundation model guided 2d mask merging. In *Proceedings of the Computer Vision and Pattern Recognition Conference*, pages 3676–3685, 2025. 1, 2, 9
- [28] Zachary Teed and Jia Deng. Droid-slam: Deep visual slam for monocular, stereo, and rgb-d cameras. Advances in neural information processing systems, 34:16558–16569, 2021.
- [29] Tao Tu, Shun-Po Chuang, Yu-Lun Liu, Cheng Sun, Ke Zhang, Donna Roy, Cheng-Hao Kuo, and Min Sun. Imgeonet: Image-induced geometry-aware voxel representation for multi-view 3d object detection. In *Proceedings of the IEEE/CVF International Conference on Computer Vision*, pages 6996–7007, 2023. 2
- [30] Jianyuan Wang, Minghao Chen, Nikita Karaev, Andrea Vedaldi, Christian Rupprecht, and David Novotny. Vggt: Visual geometry grounded transformer. In *Proceedings of the Computer Vision and Pattern Recognition Conference*, pages 5294–5306, 2025. 5, 10
- [31] Shuzhe Wang, Vincent Leroy, Yohann Cabon, Boris Chidlovskii, and Jerome Revaud. Dust3r: Geometric 3d vision made easy. In *Proceedings of the IEEE/CVF Conference on Computer Vision and Pattern Recognition*, pages 20697–20709, 2024. 2, 5, 6, 8, 10
- [32] Zhenyu Wang, Yali Li, Taichi Liu, Hengshuang Zhao, and Shengjin Wang. Ov-uni3detr: Towards unified open-vocabulary 3d object detection via cycle-modality propagation. In *European Conference on Computer Vision*, pages 73–89. Springer, 2024. 1, 2, 5, 6, 7, 9, 10
- [33] Mi Yan, Jiazhao Zhang, Yan Zhu, and He Wang. Maskclustering: View consensus based mask graph clustering for open-vocabulary 3d instance segmentation. In *Proceedings of the IEEE/CVF Conference on Computer Vision and Pattern Recognition*, pages 28274–28284, 2024. 1, 2, 3, 6, 9
- [34] Timing Yang, Yuanliang Ju, and Li Yi. Imov3d: Learning open vocabulary point clouds 3d object detection from only 2d images. *Advances in Neural Information Processing Systems*, 37:141261–141291, 2024. 1, 2, 6
- [35] Yunhan Yang, Xiaoyang Wu, Tong He, Hengshuang Zhao, and Xihui Liu. Sam3d: Segment anything in 3d scenes. arXiv preprint arXiv:2306.03908, 2023. 6, 8
- [36] Jin Yao, Hao Gu, Xuweiyi Chen, Jiayun Wang, and Zezhou Cheng. Open vocabulary monocular 3d object detection. *arXiv preprint arXiv:2411.16833*, 2024. 1

- [37] Jin Yao, Radowan Mahmud Redoy, Sebastian Elbaum, Matthew Dwyer, and Zezhou Cheng. Labelany3d: Label any object 3d in the wild. *Advances in neural information* processing systems, 2025. 1
- [38] Chandan Yeshwanth, Yueh-Cheng Liu, Matthias Nießner, and Angela Dai. Scannet++: A high-fidelity dataset of 3d indoor scenes. In *Proceedings of the IEEE/CVF International Conference on Computer Vision*, pages 12–22, 2023. 9
- [39] Dingyuan Zhang, Dingkang Liang, Hongcheng Yang, Zhikang Zou, Xiaoqing Ye, Zhe Liu, and Xiang Bai. Sam3d: Zero-shot 3d object detection via segment anything model. arXiv preprint arXiv:2306.02245, 2023. 2
- [40] Dongmei Zhang, Chang Li, Renrui Zhang, Shenghao Xie, Wei Xue, Xiaodong Xie, and Shanghang Zhang. Fm-ov3d: Foundation model-based cross-modal knowledge blending for open-vocabulary 3d detection. In *Proceedings of the* AAAI Conference on Artificial Intelligence, pages 16723– 16731, 2024. 2, 7
- [41] Jihuai Zhao, Junbao Zhuo, Jiansheng Chen, and Huimin Ma. Sam2object: Consolidating view consistency via sam2 for zero-shot 3d instance segmentation. In *Proceedings of the Computer Vision and Pattern Recognition Conference*, pages 19325–19334, 2025. 1, 2
- [42] Duo Zheng, Shijia Huang, and Liwei Wang. Video-3d llm: Learning position-aware video representation for 3d scene understanding. In *Proceedings of the Computer Vision and Pattern Recognition Conference*, pages 8995–9006, 2025. 1,
- [43] Hongyan Zhi, Peihao Chen, Junyan Li, Shuailei Ma, Xinyu Sun, Tianhang Xiang, Yinjie Lei, Mingkui Tan, and Chuang Gan. Lscenellm: Enhancing large 3d scene understanding using adaptive visual preferences. In *Proceedings of the Computer Vision and Pattern Recognition Conference*, pages 3761–3771, 2025. 1, 2
- [44] Chenming Zhu, Wenwei Zhang, Tai Wang, Xihui Liu, and Kai Chen. Object2scene: Putting objects in context for openvocabulary 3d detection. arXiv preprint arXiv:2309.09456, 2023. 2, 7
- [45] Chenming Zhu, Tai Wang, Wenwei Zhang, Jiangmiao Pang, and Xihui Liu. Llava-3d: A simple yet effective pathway to empowering lmms with 3d-awareness. *arXiv preprint* arXiv:2409.18125, 2024. 1, 2
- [46] Xiangyang Zhu, Renrui Zhang, Bowei He, Ziyu Guo, Ziyao Zeng, Zipeng Qin, Shanghang Zhang, and Peng Gao. Point-clip v2: Prompting clip and gpt for powerful 3d open-world learning. In *Proceedings of the IEEE/CVF international conference on computer vision*, pages 2639–2650, 2023. 6, 9